SPH MODELLING OF TSUNAMI WAVE IMPACT ON LOW-RISE STRUCTURES

Gede Pringgana[1], Lee S. Cunningham[2], Benedict D. Rogers[2]

This study examines the influence of low-rise structure orientations on tsunami-induced impact force. The particular focus is on low-rise structures since these often make up the majority of building stock in tsunami prone areas and are usually most vulnerable. The meshless method smoothed particle hydrodynamics (SPH) is used for simulating the tsunami flow. Multiple cube structures named A, B and C were arranged at different angles of rotation and were situated on a flat shore. Four cases were simulated with variation on the number of structures and orientation toward the tsunami direction. Case 1 comprises a single structure (SS) C without rotation (R=0°) and used as the baseline, Case 2 contains multiple structures (MS) A, B and C without rotation (R=0°), Case 3 includes multiple structures (MS) A, B and C with 30° rotation (R=30°), and Case 4 consist of multiple structures (MS) A, B and C with 45° rotation (R=45°). The simulations show that for a 2-solitary wave train the front structures generated a flow focusing effect that accelerated the bore velocity. The orientation of the multiple structures to the direction of the oncoming tsunami bore significantly affected the magnitude of the applied force, where the most effective structure orientation is provided by the 45-degree rotation. The results of this study emphasize the potential for improving tsunami resilience through appropriate positioning of structures. Importantly, such large reductions in force may provide an economic solution to building resilience in developing countries prone to tsunamis.

Keywords: structure orientation; low-rise structure; tsunami impact; smoothed particle hydrodynamics.

INTRODUCTION

Tsunamis cause severe damage to buildings, bridges and infrastructure across the affected coastal regions, as shown by major tsunami events including the 2004 Indian Ocean and the 2011 Japan tsunamis. The impact of the tsunami depends on several factors including the tsunami wave velocity and height, which are influenced by the coastal topography. For example, according to Ghobarah et al. (2006), in a largely populated and relatively flat area of Banda Aceh, Indonesia, which was the most affected area during the 2004 Indian Ocean tsunami, the maximum tsunami inundation and runup height were 4.5 km and 6 m, respectively. The runup height submerged the first storey of the low-rise structures including residential and office buildings, hotels and shops. The majority of the damages were due to the tsunami applied forces on the structure in the form of hydrodynamic pressure, scour, uplift and debris impact (Saatcioglu et al. 2005; Ghobarah et al. 2006; Mikami et al. 2012; Suppasri et al. 2012; Chock et al. 2013). In some affected areas such as in Uleele, there were a few structures that survived the tsunami including a mosque and some residential buildings. To survive tsunami impact, studies indicated various strategies can be adopted to reduce wave pressures including the use of breakaway walls and the presence of openings to allow flow through the building (Thusyanthan and Madabhushi, 2008). The orientation of a group of buildings in terms of macro-roughness elements can reduce tsunami runup on a sloping beach and inundation zone as experimentally studied by Goseberg and Schlurmann (2012) and Thomas et al. (2015). More recently, Pringgana et al. (in press) numerically explored the influence of onshore structures' orientations and arrangements due to tsunami impact using the numerical simulation technique smoothed particle hydrodynamics (SPH) and the results reveal significant reductions in total force on a structure can be achieved via strategic spatial positioning and orientation. The complex interaction between tsunami flow and structures determine the performance of structures during tsunami events.

The present study examines the influence of building orientations on the tsunami-induced hydrodynamic force. The particular focus is on low rise buildings since these often make up the majority of building stock in tsunami prone areas and are often most vulnerable. In addition to building orientation, the layout of groups of buildings and their effect on inundation flow is also presented. The most effective structure orientation is provided by the 45-degree rotation of multiple structures.

METHOD

This study uses a fully 3-D numerical modelling method to simulate the interaction of tsunami waves and building structures. The meshless method smoothed particle hydrodynamics (SPH) is used to

[1] Civil Engineering Study Program, Faculty of Engineering, Udayana University, Jalan Kampus Bukit Jimbaran, Badung, Bali, 80361, Indonesia.
[2] Department of Mechanical, Aerospace and Civil Engineering, The University of Manchester, Manchester M13 9PL, United Kingdom.

simulate the tsunami flow. SPH uses moving particles to represent the fluid and hence is ideal for the highly non-linear free-surface flow in tsunami-structure interaction. The properties of the SPH particle is influenced by its neighbouring particles located inside the compact support of the kernel which has a characteristic length denoted as the smoothing length h, as illustrated in Fig. 1.

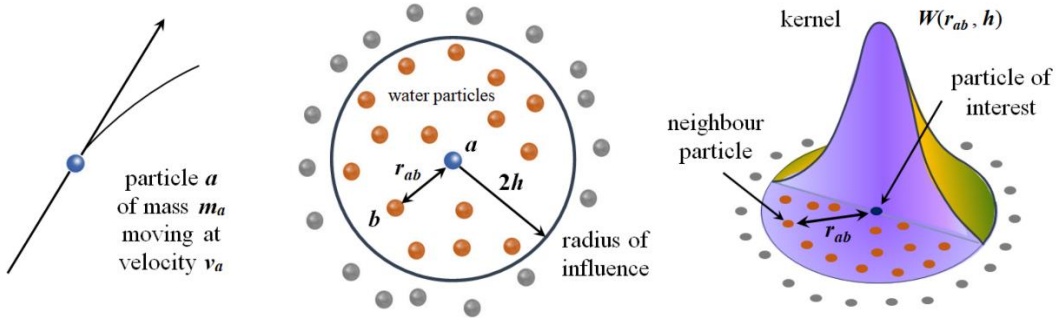

Figure 1. Diagram of the SPH smoothing kernel.

The value of a function $A(\boldsymbol{r})$ of an SPH particle located at position $\boldsymbol{r}$, can be approximated by an integral interpolant (Gomez-Gesteira et al., 2012):

$$\langle A(\boldsymbol{r})\rangle = \int_{\Omega} A(\boldsymbol{r}')W(\boldsymbol{r}-\boldsymbol{r}',h)d\boldsymbol{r}' \tag{1}$$

where $W(\boldsymbol{r}-\boldsymbol{r}',h)$ is the weighting function or kernel, h is the smoothing length that determines the radius of influence of domain Ω and $\langle ... \rangle$ denotes an approximation. In discrete notation, it can be expressed by approximation at interpolant point a, as follows:

$$A(\boldsymbol{r}_a) = \sum_b A_b \frac{m_b}{\rho_b} W_{ab} \tag{2}$$

where the subscript indicates each particle, m is the mass, ρ is density and $W_{ab} = W(\boldsymbol{r}_a - \boldsymbol{r}_b, h)$. The summation is performed over all particles b within the region of the kernel function, as depicted by Fig.1. The kernel functions comprises several properties (Monaghan 1992) such as positivity within the area of interaction, compact support, normalization and monotonic decrease with distance (Altomare et al. 2015). The efficacy of an SPH model is influenced by the selection of the smoothing kernel utilized in the model (Crespo et al. 2015). A fifth-order Wendland kernel is used in all models presented in this paper (Wendland 1995).

In this work, the weakly compressible SPH formulation is used to approximate the fluid. The weakly compressible SPH model solves the conservation of mass and momentum in Lagrangian form as

$$\frac{d\rho}{dt} = -\rho \nabla \cdot \boldsymbol{v} \tag{3}$$

$$\frac{d\boldsymbol{v}}{dt} = -\frac{1}{\rho}\nabla P + \boldsymbol{g} + \boldsymbol{\Gamma} \tag{4}$$

where $\boldsymbol{v}$ is the velocity, t is the time, ρ is the density, P is the pressure, $\boldsymbol{g}$ is the gravitational acceleration and $\boldsymbol{\Gamma}$ is the dissipative term. The continuity equation, Eq. 3, which is related with the changes of fluid particle density, can be expressed in the SPH form as follows:

$$\frac{d\rho_a}{dt} = \sum_b m_b \boldsymbol{v}_{ab} \cdot \nabla_a \boldsymbol{W}_{ab} + \delta^{SPH} \tag{5}$$

where $\boldsymbol{v}_{ab} = \boldsymbol{v}_a - \boldsymbol{v}_b$ and $\nabla_a \boldsymbol{W}_{ab}$ denotes the derivative of the smoothing kernel $\boldsymbol{W}_{ab}$ with respect to the coordinates of particle a and δ^{SPH} is the delta-SPH correction. To conserve the momentum as expressed by Eq. 4, the pressure gradient in SPH notation uses the following symetric form of gradient:

$$\frac{d\boldsymbol{v}_a}{dt} = -\sum_b m_b \left(\frac{P_a}{\rho_a^2} + \frac{P_b}{\rho_b^2} + \Pi_{ab}\right) \cdot \nabla_a \boldsymbol{W}_{ab} + \boldsymbol{g} \tag{6}$$

where Π_{ab} is the viscous forces. In weakly compressible SPH, the density fluctuation inherent in the method can be reduced by applying a delta-SPH formulation (Antuono et al. 2015; Marrone et al. 2011). A delta-SPH coefficient of 0.1 is suggested for general applications. More details about the use of SPH formulation can be found in Crespo et al. (2015). The conservation of mass and momentum in Eq. 3 and Eq. 4 are closed by an equation of state that relates pressure to density, where in weakly compressible SPH, the commonly used equation of state is

$$P = B\left[\left(\frac{\rho}{\rho_0}\right)^{\gamma} - 1\right] \tag{7}$$

where ρ_0 = 1000 kg m^{-3} is the reference density, γ = 7 for water suggested by Monaghan (1994) which proved to be efficient, , $B = c_0^2\rho_0/\gamma$, and the speed of sound at the reference density is denoted by $c_o = c(\rho_o) = \sqrt{(\partial P/\partial\rho)}|_{\rho_o}$. The maximum relative density fluctuations scale with the Mach number squared $O(M^2)$ as shown by an analysis of the compressible Navier-Stokes equations (Monaghan 1994). The use of actual speed of sound in the simulation leads to prohibitively small timestesps. Thus, to allow timesteps sufficiently large for simulations, the numerical speed of sound is modified to be at least ten times faster than the maximum fluid velocity where this restriction controls the density variation to within less than M^2 = 0.01 or 1%, maintaining the particle spacing approximately constant, and inhibits major deviation from incompressible behaviour.

The new-release open-source software DualSPHysics v5.0 used for all simulations in this study. This latest version of DualSPHysics v5.0 has been improved to better-simulate wave interactions. For this study, some key features are implemented including the use of boundary multi-layers to prevent the particle leakage and the dynamic boundary feature. Previous versions of DualSPHysics have been validated for violent wave-structure interaction modelling cases such as tsunamis as reported in Cunningham et al. (2014), Pringgana et al. (2015) and Pringgana et al. (2016). The efficacy of DualSPHysics was presented in Cunningham et al. (2014), by numerically modelling tsunami wave loading on a vertical wall following experimental investigation by Linton et al. (2013) and tsunami wave loading on a cylindrical structure as a discrete, non-orthogonal structure, based on physical testing by Zhang (2009). Good correlation between the experimental data such has been obtained in Cunningham et al. (2014), emphasizes the potential of SPH method which was then implemented in Pringgana et al. (2015) and Pringgana et al. (2016) to model a small-scale structure that was scaled up to represent a single-storey residential structure made of timber.

This present study includes numerical simulations to examine shielding and flow focusing effects on multiple structures at different angles of rotation as an idealization of low-rise residential buildings. The numerical boundary is a water tank with offshore and onshore sections. The tsunami-like waves are idealized by two consecutive solitary waves generated by paddle movement, based on the Goring (1978) equation, which were propagated along the *x*-direction from offshore to onshore. The implementation of multi-solitary waves is based on the fact that the tsunami strikes more than once. The multiple structures in the models are situated on a flat shore and consist of three cubes named A, B and C, each has the same size of 1m x 1m x 1m, as shown in Fig. 2. Two structures A and B were located at the front and structure C was located at the rear. Both front structures in theory provide shielding to the rear structure and at the same time the gap between two front structures may generate flow focusing effects to the rear structure. The distances in the domain are expressed in multiples of *D* which is equal to 1 m. The side-to-side distances between front structures are 2*D*, similar to the side-to-side distance between front and rear structures. The offshore depth of still water (h_o) is 1 m and the height of the solitary waves (*H*) is 0.5 m, resulting in a ratio of H/h_o = 0.5.

Four cases are simulated with variation on the number of structures and orientation toward the tsunami direction: Case 1: single structure (SS) C without rotation (R=0°), Case 2: multiple structures (MS) A, B, C without rotation (R=0°), Case 3: multiple structures (MS) A, B, C with 30° rotation (R=30°), and Case 4: multiple structures (MS) A, B, C with 45° rotation (R=45°). Fig. 3 shows the plan view of Case 2, Case 3 and Case 4. The water surface elevation and velocity probes are set up at the centerline of the water tank to measure the characteristics of the solitary waves and the following bores. The numerical pressure probes are located on the surfaces of the cube structures to examine impact pressure. Based on previous convergence studies involving SPH simulation of tsunami wave impact

(Cunningham et al. 2014; Pringgana et al. 2015 and Pringgana et al. 2016), the maximum particle size, d_p, should not exceed D/10 (0.1m in this case). The present study adopts a particle size of 0.04 m.

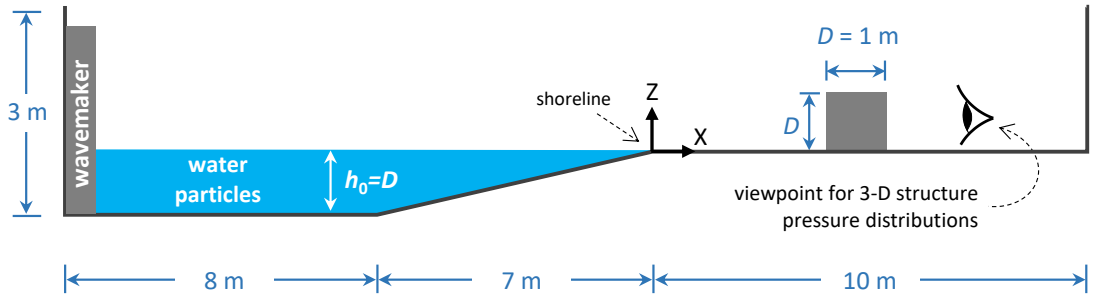

Figure 2. Side view of water tank (not to scale).

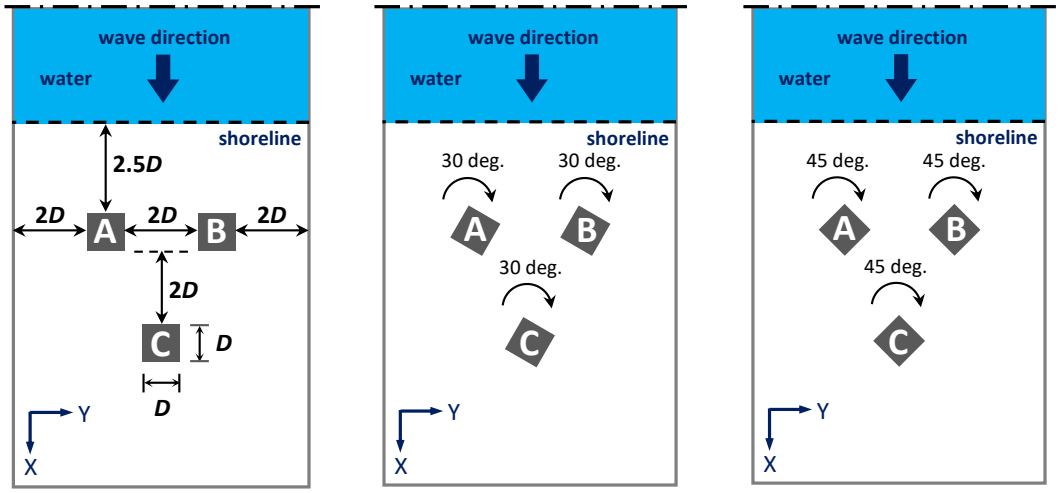

Figure 3. Plan view of 3-D SPH model with multiple structures.

Calculation of Forces

The pressure distribution on the surface of a structure is determined from numerical pressure probes distributed regularly over the surface, as illustrated in Fig. 4. The force F is then obtained by summing the pressure multipled by the area A that is impacted by the tsunami bore, following Eq. 8 and Eq. 9.

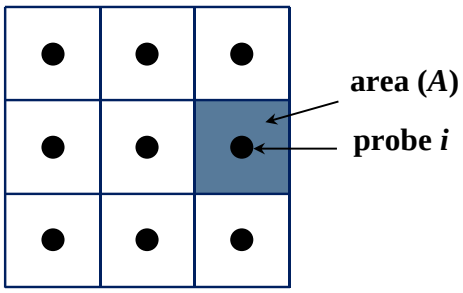

Figure 4. Example arrangement of probes on the face of a structure.

$$F_i = P_i A_i \tag{8}$$

$$F = \sum F_i = \sum_i^n (P_i A_i) \tag{9}$$

where subscript i refers to each area in Figure 4.

For a structure where the surface is perpendicular to the direction of oncoming tsunami wave, as illustrated in Fig. 5(a), the acting force F provides the force in the direction of propagation F_{total}^{x} directly because in this case only one side of the structure will be impacted by tsunami bore flow. For a clockwise-rotated structure by an angle θ, as shown by Fig. 5(b), two sides of the structure are assumed to be impacted by the tsunami bore flow. Hence, the normal forces, which are perpendicular to the sides 1 and 2 of the structure, $F_1^{\perp}$ and $F_2^{\perp}$, can be calculated using Eq. 10 and Eq. 11, respectively. The $F_1^{\perp}$ and $F_2^{\perp}$ are then resolved in the x direction to obtain the total force in x direction, F_{total}^{x} using Eq. 12 through Eq. 14. Note that in this study, only force in the x direction that are considered.

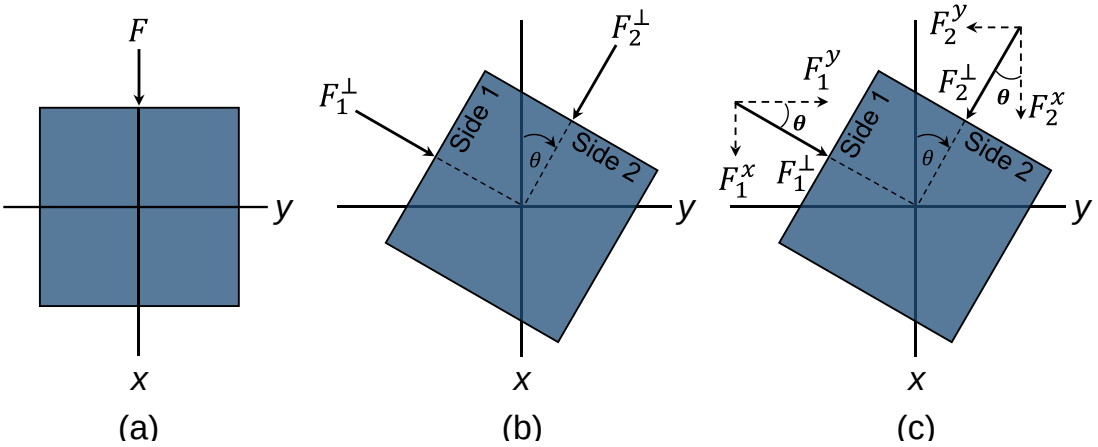

Figure 5. Plan view of the structure and resolved force in x and y directions.

a. Normal Forces on Side 1 and Side 2:

$$F_1^{\perp} = \sum_i p_i A_{1i} \tag{10}$$

$$F_2^{\perp} = \sum_i p_i A_{2i} \tag{11}$$

b. Resolved Forces in x direction due to $F_1^{\perp}$ and $F_2^{\perp}$:

$$F_1^{x} = F_1^{\perp} \sin\theta \tag{12}$$

$$F_2^{x} = F_2^{\perp} \cos\theta \tag{13}$$

c. Total Forces in x direction:

$$F_{total}^{x} = F_1^{x} + F_2^{x} = F_1^{\perp} \sin\theta + F_2^{\perp} \cos\theta \tag{14}$$

RESULTS

Contour plots of water velocity for Case 2, 3 and 4 are given in Fig. 6, these show the bore flow just after impacting the rear structure. In Fig. 6, the velocity vector is added to show the direction of bore around the structures. The offshore water surface elevation is depicted by Fig. 7, showing the propagation of two separate solitary waves. The onshore maximum velocity of the tsunami bore measured at the centerline of the water tank is shown by Fig. 8. In Fig. 8, the onshore bore velocities of all cases fluctuated before the front structures and started to increase after the bore flow passed the front structures, except for Case 1 that without front structures. Figure 6 clearly shows both the shielding and flow focusing effect of the different orientations. This is supported by the behaviour shown in Fig. 8 which indicates that the front structures generated a flow focusing effect that accelerated the bore velocity.

The total force in the x-direction applied to the surface of the rear structure C, for all modelling cases is shown in Fig. 9. It should be noted that the second wave produces a much longer duration impact,

although of similar peak force to the first impact for each of the four cases. The results show that the orientation of the multiple structures to the direction of the oncoming tsunami bore significantly affect the magnitude of the applied force. All cases with rotation show a reduction for the first wave compared to the baseline Case 1, but only Cases 3 and 4 with structure rotation are shown to lead to a significant reduction of more than 40% for the total force. The most effective structure orientation is provided by the 45-degree rotation of multiple structures.

The snapshots of pressures generated by the tsunami bore impact on the surface of the un-rotated rear structure C are depicted by Fig. 10 (a) and (b) for first and second impact, respectively. Moreover, the bore impact on the surface of the 45-degree rotated structures are illustrated in Fig. 10 (c) and (d) for the first and second bore impact, respectively. The greater extent of peak pressures across the surface of the structure is evident in Case 3 compared to Case 4.

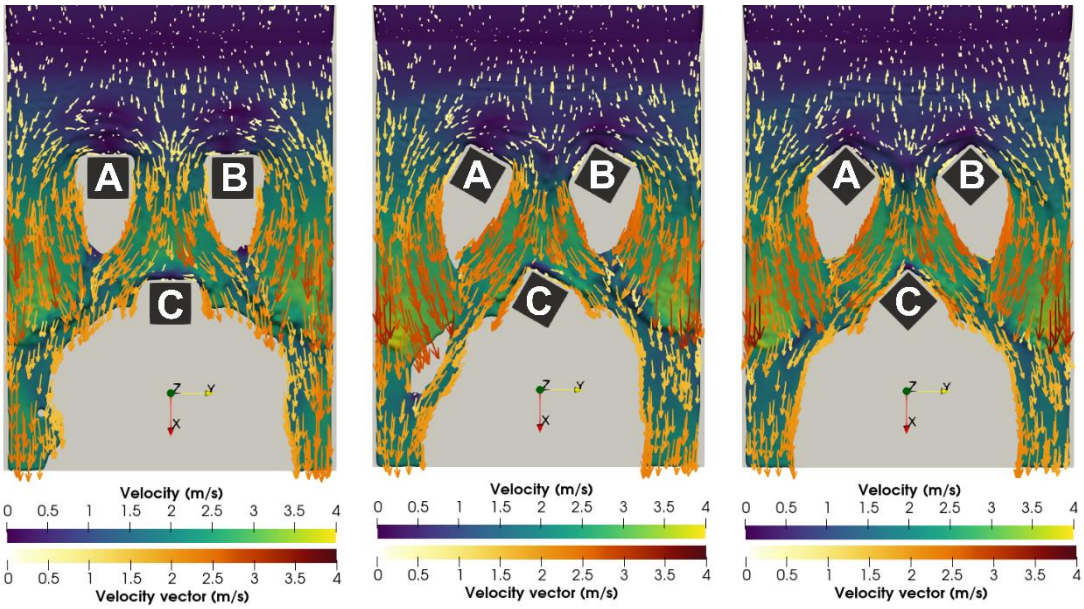

(a) Un-rotated structures (b) 30-degree rotated structures (c) 45-degree rotated structures

Figure 6. SPH model simulation of tsunami wave impacting a group of structures.

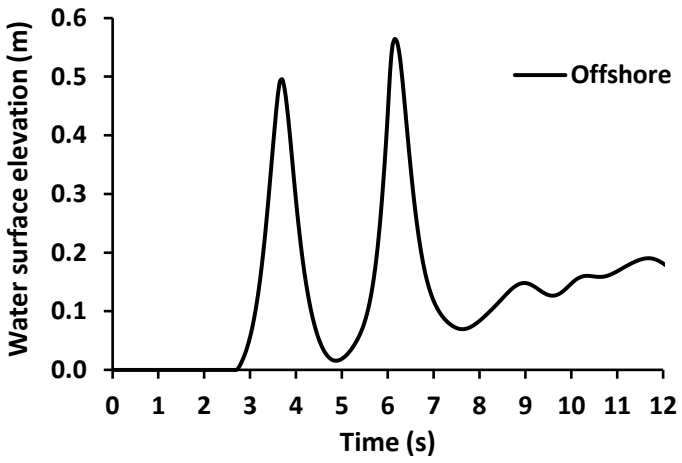

Figure 7. Offshore water surface elevation.

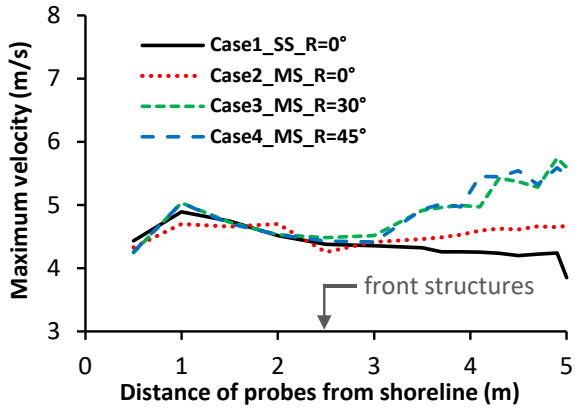

Figure 8. Onshore maximum bore velocity.

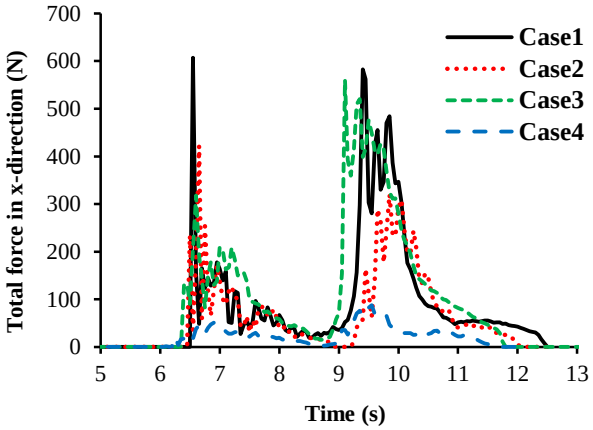

Figure 9. Total force applied on the vertical surfaces of main structure C.

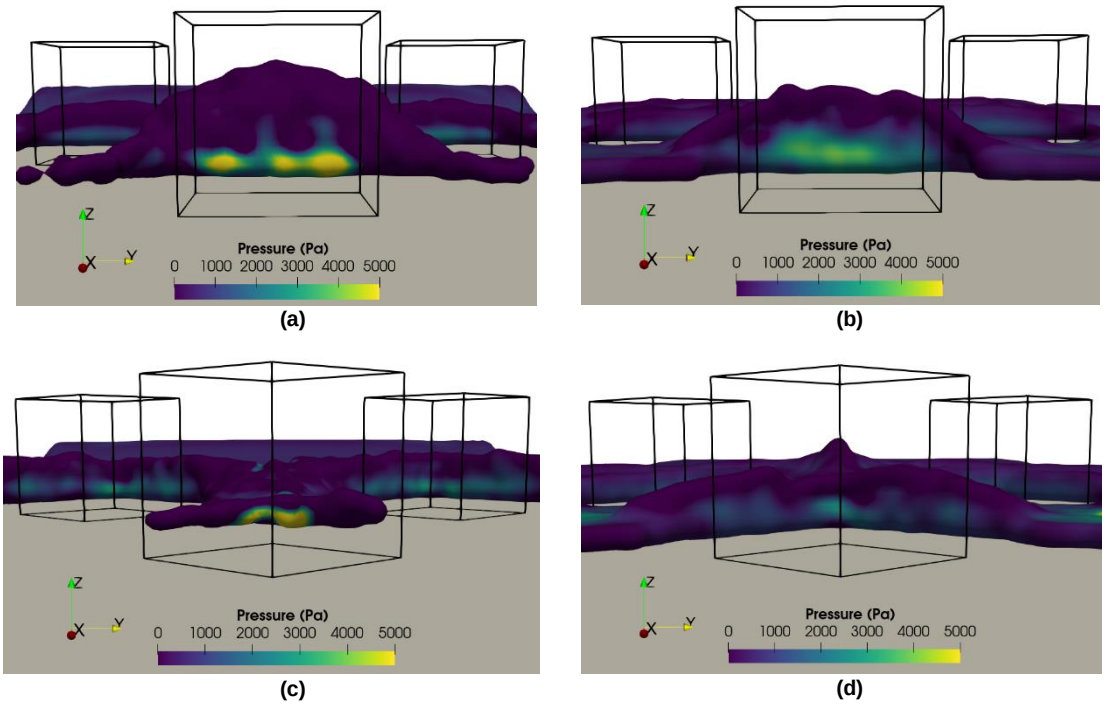

Figure 10. Tsunami bore impact on the structures' surfaces

CONCLUSIONS

The smoothed particle hydrodynamics (SPH) numerical method has been used to investigate the influence structure orientation on the forces experienced during a double-wave impact event. The results indicate the potential for improving tsunami resilience through appropriate positioning of structures. The magnitude of reduction in total force observed for multiple structures with 45° rotation could in reality mean the difference between survival and collapse. Importantly, such large reductions in force may provide an economic solution to building resilience in developing countries prone to tsunamis.

ACKNOWLEDGMENTS

The authors gratefully acknowledge the support of the Faculty of Engineering at Udayana University, Indonesia and the Department of Mechanical, Aerospace and Civil Engineering at the University of Manchester, UK.

REFERENCES

Altomare, C., Crespo, A. J. C. A. J. C., Domínguez, J. M. J. M., Gómez-Gesteira, M., Suzuki, T., & Verwaest, T. (2015). Applicability of Smoothed Particle Hydrodynamics for estimation of sea wave impact on coastal structures. *Coastal Engineering*, 96, 1–12.

Antuono, M., Marrone, S., Colagrossi, A., & Bouscasse, B. (2015). Energy balance in the δ-SPH scheme. *Comput. Methods Appl. Mech. Engrg.*, 289, 209–226.

Chock, G., Carden, L., Robertson, I., Olsen, M., & Yu, G. (2013). Tohoku tsunami-induced building failure analysis with implications for U.S. tsunami and seismic design codes. *Earthquake Spectra*, 29.

Crespo, A. J. C., Domínguez, J. M., Rogers, B. D., Gómez-Gesteira, M., Longshaw, S., Canelas, R., Vacondio, R., Barreiro, A., García-Feal, O. (2015). DualSPHysics: Open-source parallel CFD solver based on Smoothed Particle Hydrodynamics (SPH). *Computer Physics Communications*, 187, 204–216.

Cunningham, L. S., Rogers, B. D., & Pringgana, G. (2014). Tsunami wave and structure interaction: an investigation with smoothed-particle hydrodynamics. *ICE Journal of Engineering and Computational Mechanics*, 167(EM3), 126–138.

Ghobarah, A., Saatcioglu, M., & Nistor, I. (2006). The Impact of the 26 December 2004 Earthquake and Tsunami on Structures and Infrastructure. *Engineering Structures*, 28, 312–326.

Gomez-Gesteira, M., Rogers, B. D., Crespo, A. J. C., Dalrymple, R. A., Narayanaswamy, M., & Dominguez, J. M. (2012). SPHysics – development of a free-surface fluid solver – Part 1: Theory and formulations. *Computers & Geosciences*, 48(1), 289–299.

Goring, D. G. (1978). Tsunamis - The Propagation of Long Wave onto A Shelf. *W. M. Keck Laboratory of Hydraulic and Water Resources*, California Institute of Technology, CA, USA, Report Kh-R-38.

Goseberg, N., & Schlurmann, T. (2012). Interaction of idealized urban infrastructure and long waves during run-up and on-land flow process in coastal regions. *Proceedings of the Coastal Engineering Conference*.

Linton, D., Gupta, R., Cox, D., van de Lindt, J., Oshnack, M. E., & Clauson, M. (2013). Evaluation of Tsunami Loads on Wood Frame Walls at Full Scale. *Journal of Structural Engineering*, 139(8), 1318–1325.

Marrone, S., Antuono, M., Colagrossi, A., Colicchio, G., Le Touzé, D., & Graziani, G. (2011). δ-SPH model for simulating violent impact flows. *Computer Methods in Applied Mechanics and Engineering*, 200(13), 1526–1542.

Mikami, T., Shibayama, T., & Esteban, M. (2012). Field Survey of the 2011 Tohoku Earthquake and Tsunami in Miyagi and Fukushima Prefectures. *Coastal Engineering Journal*, *54*, 1–26.

Monaghan, J. J. (1994). Simulating Free Surface Flows with SPH. *Journal of Computational Physics*, 110(2), 399-406.

Pringgana, G., Cunningham, L. S., & Rogers, B. D. (in-press). Influence of Orientation and Arrangement of Structures on Tsunami Impact Forces: a numerical investigation with Smoothed Particle Hydrodynamics. *ASCE Journal of Waterway, Port, Coastal, and Ocean Engineering*.

Pringgana, G., Cunningham, L. S., & Rogers, B. D. (2015). SPH modelling of tsunami-induced bore and structure interaction using DualSPHysics. *Proceedings of the 23rd UK Conference of the Association for Computational Mechanics in Engineering 8 – 10 April 2015, Swansea University, Swansea.*

Pringgana, G., Cunningham, L. S., & Rogers, B. D. (2016). Modelling of tsunami-induced bore and structure interaction. *Proceedings of the Institution of Civil Engineers-Engineering and*

Computational Mechanics, 169(EM3), 109–125.
Saatcioglu, M., Ghobarah, A., & Nistor, I. (2005). Effects of the December 26, 2004 Sumatra Earthquake and Tsunami on Physical Infrastructure. *ISET Journal of Earthquake Technology*, 42, 79–94.
Suppasri, A., Shuto, N., Imamura, F., Koshimura, S., Mas, E., & Yalciner, A. C. (2012). Lessons Learned from the 2011 Great East Japan Tsunami: Performance of Tsunami Countermeasures, Coastal Buildings, and Tsunami Evacuation in Japan. *Pure and Applied Geophysics*, 170(6), 993–1018.
Thomas, S., Killian, J., & Bridges, K. (2015). Influence of Macroroughness on Tsunami Loading of Coastal Structures. *Journal of Waterway, Port, Coastal and Ocean Engineering*, *141*(1), 1–14.
Thusyanthan, N. I., & Madabhushi, S. P. G. (2008). Tsunami wave loading on coastal houses: a model approach. *Proceedings of the ICE - Civil Engineering*, 161(2), 77–86.
Wendland, H. (1995). Piecewise polynomial, positive definite and compactly supported radial functions of minimal degree. *Advanc. Comput. Math.*, 4(1), 389–396.
Zhang, W. (2009). *An Experimental Study and A Three-Dimensional Numerical Wave Basin Model of Solitary Wave Impact on A Vertical Cylinder*. *School of Civil and Construction Engineering*. Oregon State University.